



UNIVERSITY OF LEEDS

This is a repository copy of *Comparison of intermolecular energy transfer from vibrationally excited benzene in mixed nitrogen–benzene baths at 140 K and 300 K*.

White Rose Research Online URL for this paper:

<https://eprints.whiterose.ac.uk/167477/>

Version: Accepted Version

Article:

Ahamed, SS, Kim, H, Paul, AK et al. (5 more authors) (2020) Comparison of intermolecular energy transfer from vibrationally excited benzene in mixed nitrogen–benzene baths at 140 K and 300 K. *The Journal of Chemical Physics*, 153 (14). 144116. p. 144116. ISSN 0021-9606

<https://doi.org/10.1063/5.0021293>

© 2020 Author(s). This article may be downloaded for personal use only. Any other use requires prior permission of the author and AIP Publishing. The following article appeared in Ahamed, S. S.; Kim, H.; Paul, A. K.; West, N. A.; Winner, J. D.; Donzis, D. A.; North, S. W.; Hase, W. L., Comparison of intermolecular energy transfer from vibrationally excited benzene in mixed nitrogen–benzene baths at 140 K and 300 K. *The Journal of Chemical Physics* 2020, 153 (14), 144116 and may be found at <https://doi.org/10.1063/5.0021293> Uploaded in accordance with the publisher's self-archiving policy.

Reuse

Items deposited in White Rose Research Online are protected by copyright, with all rights reserved unless indicated otherwise. They may be downloaded and/or printed for private study, or other acts as permitted by national copyright laws. The publisher or other rights holders may allow further reproduction and re-use of the full text version. This is indicated by the licence information on the White Rose Research Online record for the item.

Takedown

If you consider content in White Rose Research Online to be in breach of UK law, please notify us by emailing eprints@whiterose.ac.uk including the URL of the record and the reason for the withdrawal request.



eprints@whiterose.ac.uk
<https://eprints.whiterose.ac.uk/>

**Comparison of Intermolecular Energy Transfer from Vibrationally Excited
Benzene in Mixed Nitrogen-Benzene Baths at 140 and 300 K**

Sk. Samir Ahamed,¹ Hyunsik Kim,² Amit K. Paul,^{1,a)} Niclas A. West,^{3,4} Joshua D. Winner,³

Diego A. Donzis,³ Simon W. North,³ and William L. Hase²

This article may be downloaded for personal use only. Any other use requires prior permission of the author and AIP Publishing. This article appeared in Ahamed, S. S.; Kim, H.; Paul, A. K.; West, N. A.; Winner, J. D.; Donzis, D. A.; North, S. W.; Hase, W. L., Comparison of intermolecular energy transfer from vibrationally excited benzene in mixed nitrogen–benzene baths at 140 K and 300 K. *The Journal of Chemical Physics* **2020**, *153* (14), 144116 and may be found at <https://doi.org/10.1063/5.0021293>.

**Comparison of Intermolecular Energy Transfer from Vibrationally Excited
Benzene in Mixed Nitrogen-Benzene Baths at 140 and 300 K**

Sk. Samir Ahamed,¹ Hyunsik Kim,² Amit K. Paul,^{1,a)} Niclas A. West,^{3,4} Joshua D. Winner,³
Diego A. Donzis,³ Simon W. North,³ and William L. Hase²

¹Department of Chemistry, National Institute of Technology Meghalaya,
Shillong 793003, India

²Department of Chemistry and Biochemistry,
Texas Tech University,
Lubbock, Texas 79409, USA

³Department of Chemistry,
Texas A&M University,
College Station, Texas 77842, USA

⁴School of Chemistry
University of Leeds
Woodhouse Lane, Leeds, LS2 9JT, United Kingdom

^{a)}Author to whom correspondence should be addressed: amit.paul@nitm.ac.in

Abstract

Gas phase Intermolecular Energy Transfer (IET) is a fundamental component of accurately explaining the behavior of gas phase systems in which the internal energy of particular modes of molecules is greatly out of equilibrium. In this work, chemical dynamics simulations of mixed benzene/N₂ baths with one highly vibrationally excited benzene molecule (Bz*) are compared to experimental results at 140 K. Two mixed bath models are considered. In one, the bath consists of 190 N₂ and 10 Bz, whereas in the other bath 396 N₂ and 4 Bz are utilized. The results are compared to 300 K simulations and experiments, revealing that Bz*-Bz vibration-vibration (V-V) IET efficiency increased at low temperatures consistent with longer lived “chattering” collisions at lower temperatures. In the simulations, at the Bz* excitation energy of 150 kcal/mol, the averaged energy transferred per collision, $\langle \Delta E_c \rangle$, for Bz*-Bz collisions is found ~2.4 times larger in 140 K than in 300 K bath, whereas this value is ~1.3 times lower for Bz*-N₂ collisions. The overall $\langle \Delta E_c \rangle$, for all collisions, is found to be almost two times larger at 140 K compared to the one obtained from the 300 K bath. Such an enhancement of IET efficiency at 140 K is qualitatively consistent with the experimental observation. However, the possible reasons for not attaining a quantitative agreement are discussed. These results imply that the bath temperature and molecular composition as well as the magnitude of vibrational energy of a highly vibrationally excited molecule can shift the overall time scale of rethermalization.

I. Introduction

Understanding and accurately modelling collisional intermolecular energy transfer (IET) is important for characterizing reaction rates in nonequilibrium environments, such as photoinitiated reactions, high temperature combustion systems, and after super/hypersonic shock waves.¹ This is especially important in systems where IET rates are comparable to chemical reaction rates.² Studying IET in nonequilibrium systems has often been performed by monitoring the efficiency of energy transfer of a vibrationally excited molecule of interest to relatively colder bath molecules.³⁻⁹ These studies often involved measuring the average energy transferred per collision, $\langle \Delta E_c \rangle$.⁴ Previous studies have shown a strong dependence on the size of a bath molecule for the relative efficiency of deactivating collisions.^{10,11} As a result of intermolecular interaction, large bath molecules may stay close to a high energy donor for longer periods of time, leading to multiple energy exchange events between the bath and donor molecules. These multiple interactions result in more efficient IET compared to collisions with small bath molecules.⁵ IET rates also strongly depend on the total number of available pathways for vibration-vibration (V-V) and vibration-rotation/translation (V-R/T) energy transfer for a given molecular collision pair.^{9,12}

Non-equilibrium between Boltzmann distributions of different types of molecular motion exists in supersonic and hypersonic gas flow fields and is known as Thermal Non-Equilibrium (TNE).¹³⁻¹⁶ TNE is often generated by shock waves and in gas expansion since, in these examples, the gas in the flow experiences a sharp change in pressure before there are enough molecular collisions to re-thermalize different types of molecular internal energy. The rate of re-equilibration of molecular translation, rotation, vibration, and electronic excitation does not occur on the same time scales and often IET can occur over the length scale of a flow field, such as over the body of

a hypersonic vehicle. Previous work has shown that this IET can modify macroscopic flow properties, like turbulent fluctuations in the velocity for flow fields.¹⁷⁻²³

Turbulence in supersonic and hypersonic boundary layers is often caused by acoustic fluctuations in a flow field.^{17,18} It has been demonstrated that if molecules in the flow can absorb the acoustic energy through IET of the correct magnitude and time scale, then the onset of transition to a turbulent flow field will be delayed.²² It is favorable in many supersonic and hypersonic flow fields to delay the transition from a laminar flow field to a turbulent flow field. Turbulence in flow fields around supersonic and hypersonic vehicles increases drag and rate of heating of the vehicle. This requires more expensive vehicle exteriors that can either withstand the increased heat or sacrificially ablate when they become too hot in order to protect the interior of the vehicle.

It is not known to what extent TNE can be utilized to modify acoustic fluctuations that cause turbulence in supersonic and hypersonic boundary layers, but several studies have begun to connect TNE and the modification of turbulence.¹⁷⁻²² The first studies to examine the role of TNE in modifying turbulence focused on delaying turbulent transitions in hypersonic boundary layers by addition of varying percentages of CO₂ into the flow fields.¹⁷⁻²¹ Some of these studies examined flow fields with CO₂ pre-mixed into the gas while others examined the effect of injecting CO₂ into the boundary layer of a hypersonic vehicle.

Since the rate that CO₂ was able to absorb acoustic fluctuations in flow fields caused the delay of transition to turbulence, studies were extended to the injection of other types of molecules into the same flow fields.²² The injection of He, N₂, and C₄F₈ into the supersonic flow field by Schmidt et al.²² demonstrated that the onset of transition to turbulence was increased in the flow field with He injection and delayed in the flow field with C₄F₈ injection as compared to a flow

field with N_2 injection. Therefore, tuning molecular factors that change the rate and magnitude of IET like molecular weight and number of vibrational modes were shown to allow for determination of the right rate of IET to modify the transition to turbulence in this flow field. This shows that there are optimal IET rates for absorbing specific frequencies of acoustic fluctuations and therefore, the ability to tune IET for diverse flow field conditions is desirable. Details of IET rates can also have a profound effect on fully developed turbulent flows, altering both turbulent fields as well as average distributions of energy across molecular modes²³ and their spectral distributions.¹³ This was found to depend, among other things, on the ratio of IET and flow time scales. TNE has also been found to affect the decay of turbulent flows in the experimental work of Fuller et al.,¹⁵ and later reproduced and explained by simulations¹⁶ which found that the interaction of TNE and turbulence depends on both the degree of TNE and the disparity of IET and time scales. This provides venues for both energy management and flow control in hypersonic applications.

Classical chemical dynamics simulation models have been developed to study IET from a vibrationally excited molecule in a bath of molecules,^{9-12,14,24-45} e.g. N_2 bath.^{14,38-40} With these simulation models, IET may be studied for mixed baths to provide insights into the dynamics associated with turbulence for multiple gases in a flow field. In recent work,⁶ IET was studied for a vibrationally excited benzene molecule, $C_6H_6^*$, in a mixed N_2 and C_6H_6 bath at 300 K, since unexcited C_6H_6 remains in experiments where $C_6H_6^*$ is generated with UV light. It was found that $C_6H_6-C_6H_6^*$ vibration-to-vibration (V-V) IET is a key process for vibrational re-thermalization following excitation. V-V pathways for $C_6H_6-C_6H_6^*$ can result in significantly more efficient rates of IET than models that only consider $N_2-C_6H_6^*$ IET pathways.^{5,7,12} Equilibration was found to be slow for $C_6H_6^*$ in the N_2/C_6H_6 bath. For a 1 atm bath pressure and at 10^{-7} sec, there were four

distinct temperatures, i.e., a rotation-translation (RT) temperature for $C_6H_6^*$ and the N_2/C_6H_6 bath, a N_2 vibration temperature, and different vibration temperatures for $C_6H_6^*$ and the bath C_6H_6 .

In the work presented here, the above simulation for $C_6H_6^*$ vibrational relaxation in the N_2/C_6H_6 bath at 300 K is extended to consider a much colder bath at 140 K. Of interest is to determine how the IET dynamics may vary in a much colder bath which is relevant to the temperatures studied in supersonic and hypersonic wind tunnels in which TNE is most often studied by aerospace engineers in ground-based blow down facilities. The 140 K simulation results are compared with the results of an experimental study at 140 K.⁴⁶

II. Simulation Method

N_2/N_2 , C_6H_6/C_6H_6 , and N_2/C_6H_6 intermolecular potentials were required for the simulations. The same potentials were used, as used in previous simulations, and are only briefly described here. They are written as sums of 2-body potentials. The N_2/N_2 potential was developed from MP2 calculations extrapolated to the CBS limit.³⁸ The C_6H_6/C_6H_6 potential is represented by the Optimized Potentials for Liquid Simulations (OPLS) model.⁴⁷ The OPLS potential gives an overall good description of the benzene-benzene interaction.⁴⁸ The geometry for global potential energy minima of benzene-dimer is tilted-T, which is in excellent agreement with CCSD(T)/CBS calculations.^{48,49} The OPLS Bz-Bz center-of-mass distance is 4.93 Å, whereas the CCSD(T)/CBS value is 4.96 Å. Moreover, the energy that OPLS model gives for the potential energy minimum is -2.32 kcal/mol compared to the CCSD(T)/CBS value of -2.84 kcal/mol. The N_2/C_6H_6 2-body potentials are written as $V(r) = A \exp(-Br) + C/r^n + D/r^m$. The values of the parameters A, B, C, D, n, and m for the N_2/C_6H_6 C-N and H-N interactions were assumed to be the same as those for the azulene + N_2 potential, developed from SCS-MP2/ 6-311++G** calculations.⁴⁰ The N_2

intramolecular potential was represented by a Morse function, with parameters taken from experiment.⁵⁰ The benzene intramolecular potential was represented by C-C and C-H Morse stretches, C-C-C and C-C-H harmonic bends, C-C-H harmonic wags, and torsions, and is the potential used in previous studies of Na⁺ interacting with benzene.^{51,52} The potential gives benzene vibrational frequencies in good agreement with experiment.⁵³

Three different simulations were performed for the results presented here. One was performed to model experiments in which C₆H₆ constitutes 1.25% of the C₆H₆-N₂ system, approximately 16% - 30% of the C₆H₆ molecules were vibrationally excited, and the bath was initially at 140 K. To represent these experiments, a simulation model was used in which the system consists of 396 N₂ and 3 C₆H₆ bath molecules, and 1 C₆H₆ molecule vibrationally excited. Thus, the simulation system was 1% C₆H₆, with 25% of the C₆H₆ molecules vibrationally excited. The initial bath temperature for this simulation was 140 K. To compare this simulation with the previous C₆H₆-N₂ bath simulation at 300 K,⁶ two additional simulations were performed. For each, the system consisted of 1 excited C₆H₆ molecule, 0 unexcited bath C₆H₆ molecules, and baths of 400 and 399 N₂ molecules at 300 and 140 K, respectively.

To achieve the binary/single collision limit for comparison with experiments, the bath density was chosen as 40 kg/m³ or 16.2 atm which was found to be the binary/single collision limiting density for C₆F₆ + N₂ simulations.^{38,39} Due to the fact that C₆H₆ is a smaller molecule than C₆F₆, and also that there is a very small percentage of C₆H₆ in the bath, the binary/single collision limiting density is expected to be achieved at 40 kg/m³ or higher density. Performing the simulations in the binary/single collision limit allows extrapolation of the simulation results to lower densities/pressures. However, such extrapolation may not be very accurate in the case when the possibility of complex formation among the molecular species present in the system is there.

Such a possibility may reduce with lowering the bath pressure and that may lead to different IET dynamics.

The simulations were performed with the same methodology as described for previous intermolecular energy transfer bath simulations.^{14,38-42} A vibrational energy of 148.1 kcal/mol was first added to the one excited C₆H₆* molecule to model the experimental 193 nm laser excitation and subsequent internal conversion.^{6,46} This energy was added randomly with classical microcanonical normal mode sampling,^{54,55} as implemented in a modified version³⁸ of the general chemical dynamics computer code VENUS.⁵⁶ Translational and rotational energies for 140 K or 300 K were then added randomly from a Boltzmann distribution at those corresponding temperatures to vibrationally excited C₆H₆*. With initial conditions for C₆H₆* chosen, the next step was to equilibrate the bath around C₆H₆* by placing it at the center of the simulation box with its coordinates and momenta fixed. An MD simulation was then performed to thermally equilibrate the bath to the desired temperature (i.e. 140 K or 300 K), using periodic boundary conditions and nearest neighbor updating to enhance the simulation. At the end of this equilibration, the desired initial temperature for the vibration, rotation, and center-of-mass translation degrees of freedom for bath molecules was verified. To illustrate this equilibration, consider the simulation bath with 396 N₂ molecules and 3 C₆H₆ molecules at 140 K. After equilibration, the average center-of-mass translation energy for each N₂ and C₆H₆ molecule was $3RT/2 = 0.41$ kcal/mol, the average rotational energy of each N₂ and C₆H₆ molecule was $RT = 0.28$ kcal/mol and $3RT/2 = 0.41$ kcal/mol, respectively, and the average vibration energy of N₂ and each mode of C₆H₆ was $RT = 0.28$ kcal/mol. These are the proper equilibrium average energies, which match the equipartition model.

With the above random initial conditions for $C_6H_6^*$ and the bath, a trajectory was then calculated for 3 ns to study intermolecular energy transfer from $C_6H_6^*$ to the bath. To obtain results which could be compared with experiments, averaging was performed by calculating an ensemble of 39 trajectories, with random initial conditions. In a previous similar simulation for $N_2 + C_6F_6$ intermolecular energy transfer,³⁸ 48 trajectories gave statistically the same result as found for 96 trajectories. A simulation with only 24 trajectories gave semi-quantitative results.

III. Simulation Results

A. Atomistic dynamics and molecular energies for the N_2/C_6H_6 bath simulation

1. Complexes of the benzene molecules

In the simulation with $C_6H_6^*$ in the N_2/C_6H_6 bath at 140 K, the center-of-mass distances between the benzene molecules were monitored to study the possibilities of dimer, trimer, and tetramer long-lived collision complex formation between the benzene molecules. There were four benzene molecules, 1 excited and 3 unexcited. In Figs. 1 and 2, distances between the benzene molecules are plotted versus time for 2 trajectories. The excited benzene molecule is Bz1 and the other three Bz2, Bz3, and Bz4, and there are 6 center-of-mass distances between these molecules. Two simultaneous criteria were used to identify complex formation between Bz molecules: i.e. the distance between the centers-of-mass of two Bz molecules is less than 10 Å (the equilibrium distance between Bz molecules is 4.93 Å for the Bz-dimer);⁴⁸ and the two Bz molecules retain a distance less than 10 Å for at least 10 ps. The orientation averaged potential energy curve as done in a previous work⁴⁸ showed a potential energy of -0.039 kcal/mol when the centers-of-mass separation between two Bz is 10 Å (see Fig. S2 with a related discussion in the supporting information). The period for the Bz---Bz intermolecular harmonic stretching vibration

is 0.5 ps for the Bz-dimer. However, the lowest normal mode frequency of Bz-dimer is 6.4 cm^{-1} , corresponding to a vibrational period of ~ 5 ps. For dimer formation, a reasonable time criterion could be two Bz-Bz vibrational periods. Moreover, fitting the orientation averaged Bz-Bz intermolecular potential energy curve to a Morse function of the form $D_e[1-\exp(\beta(r - r_0))]^2$ provides $D_e = 0.62 \text{ kcal/mol}$, $\beta = 2.88 \text{ \AA}^{-1}$, and $r_0 = 6.58 \text{ \AA}$. With the help of these parameters, the Bz-Bz vibrational period is obtained as ~ 1 ps at the orientation averaged potential energy of -0.05 kcal/mol . Therefore, the selection of 10 ps as a criterion for dimer formation is at least 2 times larger than both the Bz-dimer vibrational frequency as well as than any of the Bz vibrational frequencies. Fig. 1 is a plot of the 6 Bz-Bz distances for the trajectory with a minimum amount of complex formation, while Fig. 2 is the plot for the trajectory with the maximum amount of complex formation.

Averaged over the 39 trajectories and with the criteria for benzene complex formation given above, the average time a 3,000 ps trajectory spent as a complex was 612 ps. Thus, 20.4% of the time, the trajectory consisted of a benzene complex. The percentage of time the complex was a dimer was 17.8%, while the percentages as a trimer and tetramer were much smaller and 2.25% and 0.34%, respectively. When only complexes involving the excited benzene (Bz1) are considered, these percentages became 7.90% as total benzene complexes, 6.72% as a dimer, 1.01% as a trimer, and 0.17% as a tetramer. For the sample trajectory depicted in Fig. 1, the total percentage of complex formation was 7.06 % and all are dimer, while in Fig. 2, the total percentage of complex formation was 37.1%. Out of this, 13.8% was a dimer, 11.7% was a trimer, and 11.6% was a tetramer formation.

2. Molecular energies versus time

Average energies of $C_6H_6^*$ and the N_2 and C_6H_6 bath molecules, for the 140 K N_2/C_6H_6 bath simulation, are plotted versus time in Figs. 3 and 4. Fig. 3 gives the $C_6H_6^*$ total energy, while individual translational, rotational, and vibrational energies of the bath molecules are given in Fig. 4. For a C_6H_6 bath molecule, the average vibrational energy for one mode of the molecule is given, which equals the average vibrational energy of a C_6H_6 bath molecule divided by 30, the number of vibrational modes. While IET efficiency from different C_6H_6 modes has been previously shown to not be equal,⁵⁷ this method of calculating the per mode vibrational energy allows for comparison with individual energies of rotational and translational modes of the bath. In the following, average energies are given for the 39 trajectories, with uncertainties standard deviations of the mean. For a N_2 bath molecule, the initial average translation, rotation, and vibration energies, i.e. $\langle E_{trans} \rangle$, $\langle E_{rot} \rangle$, and $\langle E_{vib} \rangle$, are 0.416 ± 0.003 , 0.278 ± 0.002 , and 0.276 ± 0.002 kcal/mol, respectively, and at the 3 ns conclusion of the trajectories these average energies are 0.470 ± 0.003 , 0.313 ± 0.003 , and 0.277 ± 0.002 kcal/mol. Within statistical uncertainty, the average initial temperature for translation, rotation, and vibration are each 140 K, and at the conclusion of the trajectories the average temperatures for these respective degrees of freedom are 158 ± 1 , 157 ± 2 , and 140 ± 1 K. The heating of translation and rotation is similar, while there is no energy transfer to N_2 vibration, which is consistent with the energy partitioning in similar previous calculations which had an initial bath temperature of 298 K.³⁸

For the benzene (Bz) bath molecule, in the N_2/C_6H_6 bath, the initial $\langle E_{trans} \rangle$ and $\langle E_{rot} \rangle$ are 0.445 ± 0.03 and 0.433 ± 0.04 kcal/mol, respectively, and the average energy in one vibration mode of Bz, $\langle E_{vib} \rangle$, is 0.270 ± 0.01 kcal/mol. At the 3 ns conclusion of the trajectories these average energies are 0.450 ± 0.04 , 0.560 ± 0.04 , and 1.08 ± 0.04 kcal/mol. Within statistical uncertainty, the average initial temperature for translation, rotation, and vibration are each 140 K,

and at the conclusion of the trajectories the average temperatures for these respective degrees of freedom are 150 ± 13 , 188 ± 13 , and 543 ± 20 K. There are two interesting features for the energy transfer to Bz. Energy transfer to Bz vibration is substantially more efficient than transfer to Bz translation and rotation, dynamics observed in the previous simulation of $C_6H_6^*$ relaxation in a N_2/C_6H_6 bath initially at 300 K.⁶ In addition, energy transfer to Bz rotation is slightly more efficient than transfer to Bz translation. The fluctuations in the average Bz rotational energy are much greater than those for the translational energy. Such dynamics were not observed in the previous N_2/C_6H_6 bath simulation at 300 K.

$\langle E_{trans} \rangle$ and $\langle E_{rot} \rangle$ and per mode vibrational energy $\langle E_{vib} \rangle$ of $C_6H_6^*$ versus time, for the N_2/C_6H_6 bath simulation, are given in Fig. 5. The initial $\langle E_{trans} \rangle$ and $\langle E_{rot} \rangle$ are 0.45 ± 0.05 and 0.48 ± 0.07 kcal/mol, respectively, and $\langle E_{vib} \rangle$ is 4.93 ± 0.40 kcal/mol. At the 3 ns conclusion of the trajectories these average energies are 0.49 ± 0.06 , 0.67 ± 0.14 , and 1.70 ± 0.14 kcal/mol. $\langle E_{trans} \rangle$ does not change with time, a result similar to that for a C_6H_6 bath molecule (Fig. 4 and above discussion). $\langle E_{rot} \rangle$ rapidly increases, but then decreases to a value slightly higher than that for $\langle E_{trans} \rangle$. For a C_6H_6 bath molecule, $\langle E_{rot} \rangle$ increases with time (Fig. 4). The large fluctuations in $\langle E_{rot} \rangle$, for $C_6H_6^*$ in Fig. 5, are partly due to the small number of $C_6H_6^*$ molecules in the analysis; i.e., 39, with one for each of the 39 trajectories. At the end of the 3 ns simulation, the $C_6H_6^*$ translation, rotation, and vibration temperatures are 164 ± 20 , 225 ± 47 , and 855 ± 70 K. K. The 3 ns translation, rotation, and vibration temperatures for the N_2 and C_6H_6 bath molecules, and $C_6H_6^*$, are summarized in Table I. It should be noted that a complete re-equilibration of the $C_6H_6^*$ vibration has not been achieved at 3 ns, i.e., at the termination of the trajectories. The final $C_6H_6^*$ per mode vibrational energy at 3 ns is 1.70 ± 0.14 kcal/mol, which is about 1/3 of its initial energy. The 3 ns energy of bath- C_6H_6 molecules for the same mode is 1.08 ± 0.04 kcal/mol.

The average energies of $C_6H_6^*$ versus time, for the simulations with the N_2 bath at 140 and 300 K, are plotted in Fig. 6. These results are obtained from the simulations where there is no unexcited C_6H_6 molecule in the bath. One can see from this figure that the energy transfer at 300 K bath is more efficient than that of 140 K. The translational, rotational, and vibrational temperatures of these simulations at both 140 and 300 K are obtained and compared with the ones from mixed bath simulations mentioned above. At the 3 ns conclusion of the 140 K simulations, T_{trans} and T_{rot} are 155 ± 1 and 157 ± 1 K, respectively, for a N_2 bath molecule, and 137 ± 16 and 319 ± 74 K for $C_6H_6^*$. T_{vib} for $C_6H_6^*$ is $1,974 \pm 25$ K. These temperatures, except T_{vib} , are statistically the same as those given above for the N_2/C_6H_6 bath simulation at 140 K. For the 300 K simulation of the N_2 bath, T_{trans} and T_{rot} are 316 ± 2 and 317 ± 2 K for N_2 and 310 ± 40 and 362 ± 52 K for $C_6H_6^*$. T_{vib} for $C_6H_6^*$ is $1,749 \pm 52$ K. Within statistical uncertainties, these temperatures, except T_{vib} , are the same, as found for the previous N_2/C_6H_6 bath simulation at 300 K.⁶ However, for both the 140 K and 300 K N_2 bath simulations there is some indication that T_{rot} for $C_6H_6^*$ is a bit higher than T_{trans} and T_{rot} for N_2 and T_{trans} for $C_6H_6^*$. However, better statistics are required to determine if this is indeed the case.

B. Energy transfer dynamics per collision

An important analysis from the simulations is determination of the average energy transferred per collision, $\langle \Delta E_c \rangle$, from vibrationally excited $C_6H_6^*$. $\langle \Delta E_c \rangle$ is found from the simulation $\langle E(t) \rangle$ and given by

$$\langle \Delta E_c \rangle = [d\langle E(t) \rangle / dt] / \omega \quad (1)$$

where $d\langle E(t)\rangle/dt$ is the energy transfer per unit time and ω is the collision frequency in s^{-1} . To facilitate the analysis the simulation $\langle E(t)\rangle$ are fit analytically. As found for previous simulations,^{6,48-42} the $\langle E(t)\rangle$ are well fit by the bi-exponential

$$\langle E(t)\rangle = [E(0) - E(\infty)][f_1 \exp(-k_1 t) + f_2 \exp(-k_2 t)] + E(\infty) \quad (2)$$

where $f_1 + f_2 = 1$, $E(0)$ is the initial energy of $C_6H_6^*$, k_1 and k_2 are rate constants, and $E(\infty)$ is the corresponding energy value of $C_6H_6^*$ at complete re-equilibration of the baths. The fits are shown in Figs. 3 and 6, with the fitting parameters listed in Table II, along with properties of the baths. Also included are the fitting parameters for the previous N_2/C_6H_6 bath simulation at 300 K.⁶ $\langle \Delta E_c \rangle$ in Eq. (1) includes all collisions, both those that transfer energy from and to $C_6H_6^*$.

For the simulation with the N_2/C_6H_6 bath, the collision frequency is a sum of the collision frequencies for $C_6H_6^*$ colliding with the N_2 and C_6H_6 bath molecules and is $\omega = \omega(C_6H_6^*-N_2) + \omega(C_6H_6^*-C_6H_6)$. For the N_2 bath simulations, the only collision frequency is $\omega(C_6H_6^*-N_2)$. The collision frequency for each bath component may be expressed as $\omega = \omega_P \times P$, where P is the partial pressure of the bath gas. The ω_P used here is the same as the values to interpret the experiments,³² with which the simulations are compared. These values for N_2 and C_6H_6 along with the resulting $\omega(C_6H_6^*-C_6H_6)$ and $\omega(C_6H_6^*-N_2)$ are summarized in Table III for both 140 and 300 K mixed bath simulations. The pressures used to determine the collision frequencies were those for the bath when the simulation was initiated. The partial pressures of N_2 and C_6H_6 for the 140 and 300 K mixed bath simulations are also presented in Table III. The pressure for the pure N_2 bath is 35.0 and 16.3 atm at 300 and 140 K, respectively. It is interesting to note here that the number of $C_6H_6^*-N_2$ and $C_6H_6^*-C_6H_6$ collisions in 2.4 ns of the trajectory calculation at 300 K

are ~847 and ~62, respectively, whereas these numbers for the 3 ns trajectory integration at 140 K are 1161 and ~13, respectively, yielding a higher percentage of C₆H₆*-C₆H₆ collisions at 140 K even though there was a lower percentage of C₆H₆ molecules at 140 K.

Of interest from the analysis of $\langle E(t) \rangle$, as described by Eq. (1), are the values of $\langle \Delta E_c \rangle$ for C₆H₆* energy transfer to the N₂ and C₆H₆ bath molecules; i.e., $\langle \Delta E_c \rangle_{N_2}$ and $\langle \Delta E_c \rangle_{Bz}$. Values of $\langle \Delta E_c \rangle_{N_2}$ for collisions of N₂ with C₆H₆*, at 140 K and 300 K, were determined from the simulation plots of $\langle E(t) \rangle$ in Fig. 6 and the fitting parameters in Table II. The resulting values of $\langle \Delta E_c \rangle_{N_2}$ versus $\langle E(t) \rangle$ are plotted in Fig. 7, where it is seen that $\langle \Delta E_c \rangle_{N_2}$ is significantly smaller at 140 K than 300 K. The same analysis was applied to $\langle E(t) \rangle$ versus time in Fig. 3, using the fitting parameters in Table II, to determine $\langle \Delta E_c \rangle$ versus $\langle E(t) \rangle$ for collisions of C₆H₆* with the N₂/C₆H₆ bath at 140 K. This information was given previously for the simulations at 300 K. The plots of $\langle \Delta E_c \rangle$ versus $\langle E(t) \rangle$, for the 140 K and 300 K simulations, are given in the Supporting Information. Using Eq. (A6) in the Appendix, the values of $\langle \Delta E_c \rangle$ for collisions of C₆H₆* with the N₂/C₆H₆ bath, and values of $\langle \Delta E_c \rangle_{N_2}$, values of $\langle \Delta E_c \rangle_{Bz}$ were determined for collisions of C₆H₆* with the C₆H₆ bath molecules. The values are plotted in Fig. 7, and it is seen that C₆H₆* + C₆H₆ energy transfer is much more efficient at 140 K than 300 K. The $\langle \Delta E_c \rangle_{Bz}$ at 140 K is ~11 kcal/mol, whereas the same at 300 K is ~5 kcal/mol at the excitation energy of 148.1 kcal/mol. It is to note here that in a previously done classical trajectory study⁵⁷ on Bz* + Bz single-collision energy transfer, the $\langle \Delta E_c \rangle_{Bz}$ was obtained as ~2.6 kcal/mol at Bz* excitation energy of 116.4 kcal/mol and Bz temperature of 300 K. However, it was also shown that when the rotationally frozen condition was implemented in the classical trajectory study, the chances of formation of the collisional complexes with longer lifetimes was larger, and consequently, the $\langle \Delta E_c \rangle_{Bz}$ value increased. At the same excitation energy, $\langle E(t) \rangle_{Bz^*} = 116.4$ kcal/mol, the $\langle \Delta E_c \rangle_{Bz}$ from our

simulations in Fig. 7 is ~ 3.7 kcal/mol, which could be due to the formation of more collisional complexes in the present simulation model. However, at 140 K, $\langle \Delta E_c \rangle_{Bz}$ becomes almost two times larger at $\langle E(t) \rangle_{Bz^*} = 116.4$ kcal/mol than at 300 K. In the previous classical trajectory study⁵⁸ mentioned above, the lowest Bz temperature simulated was 200 K, where $\langle \Delta E_c \rangle_{Bz}$ was found to be $\sim 4\%$ more than the one at 300 K and is ~ 2.7 kcal/mol for the down $Bz^* - Bz$ collisions. Therefore, it can be assumed that the value of $\langle \Delta E_c \rangle_{Bz}$ increases sharply when the temperature decreases from 200 K to 140 K. The possible reason for such a behavior is discussed in Section B.V.

IV. Comparison with Experiment

For comparisons with the experiments, described below, it is important to have simulation values for the average energy transferred from vibrationally excited Bz^* per collision, $\langle \Delta E_c \rangle_{Bz^*}$, versus the bath temperature. The atomistic simulation studies for the model presented here provide the details of IET dynamics, namely, effect of intermolecular potential energy parameters, energy distribution of the excited molecule, energy partitioning among center-of-mass translational, rotational and vibrational modes for the collision partners, along with the underlying the dynamics. It is also possible to identify the gateway modes of energy transfer. Overall, the simulations provide many more IET parameters than experiments which only measured the bath N_2 transient rotational/translational temperature by proxy with 1% seeded NO. Previously,⁶ a simulation was performed for Bz^* relaxation in a N_2/Bz bath at 300 K and for the current work such a simulation was performed at 140 K. However, the $\langle \Delta E_c \rangle_{Bz^*}$ vs $\langle E(t) \rangle_{Bz^*}$ simulation results do not provide a direct comparison since the composition of the N_2/Bz bath was different for the two simulations. The model for the 300 K simulation consisted of one excited benzene molecule Bz^* and 9 Bz and

190 N₂ bath molecules, to represent experiments with a N₂/Bz bath of 5% Bz and 10% of the Bz vibrationally excited.⁶ In contrast, the model for the current 140 K simulation consisted of a Bz* molecule and 3 Bz and 396 N₂ bath molecules, constituting a model that is 1% Bz, with 25% of Bz vibrationally excited. This model represents experiments at 140 K in which Bz constitutes 1.25% of the N₂/Bz system and 16% - 30% of Bz is vibrationally excited.

Although the total energy transfer from Bz*, $\langle \Delta E_c \rangle_{Bz^*}$, may not be directly compared for the 140 K and 300 K simulations, the values for energy transfer versus temperature to the N₂ and Bz bath molecules, $\langle \Delta E_c \rangle_{N_2}$ and $\langle \Delta E_c \rangle_{Bz}$, provide a means to determine how $\langle \Delta E_c \rangle_{Bz^*}$ depends on temperature. As published previously,⁶ $\langle \Delta E_c \rangle_{Bz^*} = 0.44$ kcal/mol for Bz* with an average energy $\langle E(t) \rangle_{Bz^*} = 150$ kcal/mol in the 300 K simulation. In order to compare simulated $\langle \Delta E_c \rangle_{Bz^*}$ values at 140 K and 300 K for Bz* with $\langle E(t) \rangle_{Bz^*} = 150$ kcal/mol, the bath composition at 140 K (i.e., 396 N₂ + 3 C₆H₆) was converted to the bath composition at 300 K (i.e., 190 N₂ + 9 C₆H₆) by utilizing the values of $\langle \Delta E_c \rangle_{N_2}$ and $\langle \Delta E_c \rangle_{Bz}$ in Fig. 7 for 140 K in Eq. (A6). The resulting value for $\langle \Delta E_c \rangle_{Bz^*}$ is 0.83 kcal/mol, about two times larger than the value at 300 K. The same comparison may be made for the simulation at 140 K, for which $\langle \Delta E_c \rangle_{Bz^*} = 0.18$ kcal/mol at $\langle E(t) \rangle_{Bz^*} = 150$ kcal/mol. Using the bath composition for 140 K in Eq. (A6), with values of $\langle \Delta E_c \rangle_{N_2}$ and $\langle \Delta E_c \rangle_{Bz}$ in Fig. 7 for 300 K, $\langle \Delta E_c \rangle_{Bz^*}$ is 0.12 kcal/mol, which is almost 1.5 times smaller than the value at 140 K. Values of $\langle \Delta E_c \rangle_{Bz^*}$ versus $\langle E(t) \rangle_{Bz^*}$, for the 140 K and 300 K simulations are given in Fig. S1 and, as described above, values of $\langle \Delta E_c \rangle_{Bz^*}$ may be determined for the 140 K and 300 K bath compositions at 300 K and 140 K, respectively. The resulting plots of $\langle \Delta E_c \rangle_{Bz^*}$ at 140 K and 300 K, for the 140 K and 300 K bath compositions, are given in Fig. 8 versus $\langle E(t) \rangle_{Bz^*}$. $\langle \Delta E_c \rangle_{Bz^*}$ is approximately 1.5 to 2 times larger at 140 K at all $\langle E(t) \rangle_{Bz^*}$ for both baths.

The experimental procedures were described in detail previously,^{7,46} and the experiments at 300 K were summarized in a comparison of simulation and experimental studies of Bz* relaxation in a N₂/Bz bath initially at 300 K.⁶ In the experiments, Bz* was generated by 193 nm photoexcitation and subsequent rapid internal conversion, and then Bz* collisionally relaxed in N₂/Bz baths of 300 K and 140 K initial temperatures. The transient rotational-translational temperature rise of (97.75%) N₂ in the bath was monitored by proxy via LIF rotational temperature measurements of seeded NO which comprised 1% of the bath. Seeded NO was chosen due to its quick RT-RT equilibration with N₂, a negligibly different heat capacity to N₂ (to not disturb low-temperature Laval flow fields), and the relatively high S/N obtained from LIF measurements. Temperature-dependent Bz*-N₂ and Bz*-Bz collision frequencies were calculated with Lennard-Jones parameters for Bz and N₂. For unambiguous comparison with experiment, the same collision frequencies were used to analyze the simulations. The previous comparisons of the initially 300 K experiments and simulations gave values for $\langle \Delta E_c \rangle_{Bz^*}$ in agreement and the simulations revealed the importance of Bz*-Bz vibrational energy transfer in the collisional relaxation of Bz*.

For the 140 K experiment considered here, the N₂/Bz bath consisted of 1.25% Bz and between approximately 16-30% of the Bz was estimated to have been vibrationally excited. The temperature rise of the bath reached 95% of its maximum value, ~225 K, by 10 μ s, which was calculated to have occurred over ~ 400 Bz*-N₂ and ~ 8 Bz*-Bz collisions. After ~10 μ s, the lack of any further significant observable rise in NO rotational temperature indicated that either Bz* had finished collisional relaxation or that any further relaxation occurred on a time scale which was too slow to measure in the Laval apparatus. In Fig. 8 a plot of the experimental average energy transferred per collision versus the internal energy of Bz* is given and compared with the above simulation results with similar bath composition and percentage of Bz molecules vibrationally

excited. As seen from Fig. 8, the experimental $\langle \Delta E_c \rangle_{Bz^*}$ is about 14 times larger than the simulation $\langle \Delta E_c \rangle_{Bz^*}$ at the $\langle E(t) \rangle_{Bz^*}$ of 150 kcal/mol. There is a discrepancy in final N₂ rotational temperature between the experiment and simulation. The ΔT from the experiment is about 5 times larger than that from the simulation. The possible sources of this mismatch between experimental and simulation $\langle \Delta E_c \rangle_{Bz^*}$ are addresses in the next section.

By comparing the current experimental results with those from previous studies,³² the average energy transferred per collision was found to increase with decreasing temperature below 300 K, which is opposite of the behavior observed above 300 K. The IET efficiency for the 140 K curve, where the temperature rises from 140 K to 225 K, is approximately two times larger than the IET efficiency for the temperature rise from 300 K to 610 K. Therefore, the IET rate increases more quickly per Kelvin below 300 K than it does above 300 K. A few possible origins of the more efficient energy transfer at 140 K is discussed in the next Section.

V. Importance of Bz*-Bz Transient Dimers for Vibrational Relaxation of Bz* at Low T

While the percentage of Bz molecules was up to 5.6 times lower in the 140 K experiment than in the 300 K experiments, it is important to consider whether both the extent to which Bz*-Bz and Bz-Bz collision lifetimes increases at lower temperatures due to longer lived “chattering” collisions as well as the possible formation of collisionally stabilized dimers at low temperatures, both of which would allow for more efficient Bz*-Bz IET. It may be useful to remember that, based on an orientation-averaged calculation,⁴⁸ the Bz-Bz potential energy parameters used in the simulation provide a potential energy minimum of -0.54 kcal/mol for a Bz – Bz center-of-mass separation of 6.7 Å. However, the global minimum was calculated as -2.32 kcal/mol for a tilted-T geometry. The formation of long-lived complexes in the simulations of this work are consistent

with the observations from simulations of Bernshtein et al. in which ~ 7 ps “chattering” collision complexes formed in classical trajectory calculations at 200 K (as opposed to ~ 30 fs “hit-and-run” collisions).⁵⁸ Therefore, these “chattering” collision complexes would have longer collision lifetimes at 140 K due to the lower average molecular velocities and the increased IET efficiency can be explained by multiple energy transfer events during each “chattering” collision complex.

Along with the $\text{Bz}^*/\text{Bz} - \text{Bz}$ complex formations, one could also expect the possible formation of $\text{Bz}^*/\text{Bz} - \text{N}_2$ complexes during the simulation at low T . If such complexes were formed, the IET could be enhanced to some extent. Many trajectories were analyzed with a similar method to evaluate the presence of Bz dimers, i.e., by monitoring the center-of-mass distance between Bz and N_2 . Several random N_2 molecules were selected from the bath to calculate the center-of-mass distance with all four Bz molecules. However, there is no evidence of any $\text{Bz}^*/\text{Bz} - \text{N}_2$ complex formation in the simulation. An orientation average potential energy versus center-of-mass distance as utilized for $\text{Bz} - \text{Bz}$ complexes, was also calculated for $\text{Bz} - \text{N}_2$ interactions using the potential energy parameters used in the simulation (see Fig. S3 of SI). The minimum energy was obtained as -0.24 kcal/mol, which is more than two times larger than that of $\text{Bz} - \text{Bz}$. Moreover, the global minima for the $\text{Bz} - \text{N}_2$ system was only -0.75 kcal/mol and is much smaller than -2.32 kcal/mol as that of Bz dimer. Thus, $\text{Bz} - \text{N}_2$ interaction is much weaker than $\text{Bz} - \text{Bz}$ interaction, which perhaps the reason for the $\text{Bz} - \text{N}_2$ complexes not being formed in the simulation.

In order to avoid the formation of collisionally-stabilized benzene dimers in experiments, experimental conditions were chosen in a regime in which no significant formation of collisionally-stabilized benzene dimers would have been able to occur on the time scale of the 140 K experiment according to experimental rate coefficients for the formation of collisionally-

stabilized benzene dimers measured by Hamon et al.⁵⁹ (i.e., the reason that a lower [Bz] was utilized for the 140 K experiment than for the 300 K experiments). The experimental conditions were also similar to previous NO quenching experiments by Bz.⁶⁰ Since benzene has a melting point of 278.68 K and is a solid at 140 K given a long enough time scale, experiments were carried out such that the Bz/N₂/NO gas mixture was cooled and measured quickly enough at a low enough pressure that negligible formation of collisionally-stabilized benzene dimers would have been formed (where collisions with other bath species occurred on order of every 100 ns during a 10 μ s experiment). However, if this assumption is untrue, then it is one possible explanation for the dramatically increased IET observed in the 140 K experimental results. A recent study on the simulated IET dynamics of C₆H₆-C₆F₆^{*} complex in N₂ bath showed that the IET efficiency increased significantly for aromatic complexes.⁶¹ At the excitation energy of 67 and 125 kcal/mol, the $\langle \Delta E_c \rangle$ was obtained as ~2.7 and ~4.8 kcal/mol, respectively, for the N₂ bath density of 20 kg/m³. In comparison, for an excitation energy of 104 kcal/mol, C₆F₆^{*} gave a $\langle \Delta E_c \rangle$ of ~2.7 kcal/mol at the same bath density.^{38,39} If collisionally-stabilized benzene dimers (Bz-Bz) were present during the experiments, then some Bz^{*}-Bz IET would not have needed to wait for the collision of a Bz^{*} monomer and a Bz monomer if dimers were excited by the 193 nm light. In this case, excited Bz dimers as well as Bz oligomers would have occurred more often than originally anticipated, both of which would have led to increase IET. Based on the Hamon's dimerization rate coefficient which was measured at a much lower pressure,⁵⁹ the percent of complex at 123 K would be much less than 1% during the current 140 K simulation time of 3 ns. There is negligible percentage of Bz-Bz complex formed in the simulation with vibrational temperature below 300 K and no complex with vibrational temperature similar to the overall bath temperature. Alternatively, if the dimers with lifetime 50 ps or more are taken, the percentage of those dimers formed in the

simulation is about 2% with respect to the total simulation time. Thus, considering collisionally stabilized Bz-Bz dimers and not just Bz-Bz collisional complexes, those numbers are more-or-less consistent with that of Hamon's.

Although the IET dynamics are non-statistical within the simulation time scale, one may consider that at infinite time, the final bath temperature becomes 186 K with an overall ΔT of 46 K. The rotational ΔT of N_2 at the termination of trajectory at 3 ns in the current 140 K simulation is 17 K. Therefore, at 3 ns, the simulation is about 37 % of the way to a hypothetical complete equilibration. On the other hand, the N_2 rotational ΔT is obtained as 85 K from the experiment. If it is assumed that the experiment is completely re-equilibrated with respect to the translation/rotational modes of N_2 then, the experimental ΔT is twice as large as in the simulation. The observed differences in the total magnitude of the N_2 temperature rise and IET efficiency from the simulations and the experiments could have arisen from several sources. There are several potential sources of experimental error (discussed in more detail in the Supporting Information) which cannot individually account for all of the differences including: error in the initial [Bz], the [Bz*] generated at 140 K, 193 nm multiphoton absorption of Bz, and possible enhanced absorption of 193 nm light by Bz dimers. More likely experimentally based sources of error that may explain the difference between experiment and simulations are whether NO behaves sufficiently like the bath N_2 molecules at low temperatures such that NO can still act as a proxy for determining N_2 IET properties or also if it is possible for NO to quench electronically excited Bz more efficiently at low temperatures. The possible sources of error in the simulation (discussed in more detail in the Supporting Information) could be from intermolecular potential energy parameters and trajectory initial conditions. However, any errors from the simulation method utilized are not likely to have caused the magnitude of difference between simulated and experimental results.

VI. Conclusions

Classical trajectory calculations at 140 K were performed with one vibrationally excited benzene molecule having an excitation energy of 148.1 kcal/mol undergoing collisional re-equilibration in a benzene/N₂ bath in order to determine the time-dependent internal energy partitioning between internal modes of the Bz* molecule, the Bz bath molecules, and the N₂ bath molecules. Two different baths, one with 190 N₂ + 9 Bz and another with 396 N₂ + 3 Bz were considered in these simulation studies. These simulations were performed since previously only two (RT) modes of the bath N₂ molecules had been examined experimentally by proxy via NO LIF temperature measurements, and the experiment did not directly give information about the other molecular modes during the re-equilibration of Bz*.⁴⁶ Additionally, the 140 K bath experiment and simulations were compared to 300 K experiments and simulations in order to examine the temperature dependence of the IET processes.^{6,7}

At 140 K, it was found that Bz*-Bz V-V IET was highly efficient, which is consistent with previous temperature-dependent Bz*-Bz classical trajectory calculations.⁵⁸ It was previously found that longer-lived, multiple-IET-event, “chattering” Bz*-Bz complexes were formed which increase the IET efficiency as the lifetime of the complexes increased at lower temperatures. For the bath with 396 N₂ and 3 Bz, the average energy transferred per collision $\langle \Delta E_c \rangle$ was found to be ~12 kcal/mol for the Bz*-Bz collisions at $\langle E(t) \rangle_{\text{Bz}^*}$ of 150 kcal/mol and the bath temperature of 140 K. This value is only about 5 kcal/mol at 300 K. In the present simulations, benzene dimer and trimer formation were quantified at 140 K in order to estimate the effect of chattering collisions on IET efficiency. The partitioning of energy of R/T modes in these simulations was also consistent with the work of Oref et al. which showed minimal V-R/T IET in Bz*-Bz collisions.

In Bz*-N₂ IET, V-RT IET dominated with negligible V-V IET observed during the duration of the simulations. The Bz*-N₂ V-RT IET per collision was lower in magnitude at 140 K than at 300 K, consistent with an impulsive collision model. For the bath with 396 N₂ and 3 Bz, $\langle \Delta E_c \rangle$ was found to be ~0.050 kcal/mol for the Bz*-N₂ collisions at $\langle E(t) \rangle_{\text{Bz}^*}$ of 150 kcal/mol and the bath temperature of 140 K. This value is about 0.064 kcal/mol at 300 K. The overall $\langle \Delta E_c \rangle$ resulted from all the collisions was found about two times higher at 140 K than at 300 K. However, the experimental value is about 10 times larger than the result obtained from the simulation. A few of the most likely possible reasons for that could be a higher Bz* concentration in the experiment than in the simulation and/or the dipole-quadrupole interaction of Bz*-NO at low temperature. The latter may lead to a remarkable enhancement of energy transfer to the bath. Therefore, the overall increased rethermalization of Bz* observed at 140 K in experiment and simulations was due to the increase in Bz*-Bz V-V IET and not due to other IET processes for these percentages of excited and unexcited Bz molecules in N₂. Therefore, the time scale of collisional relaxation of Bz* can be tuned in gas systems by varying the molecular composition of the bath. The ability to tune IET in gas systems could allow for the tuning of the onset of turbulence in the gas around hypersonic vehicles allowing for more efficient hypersonic vehicle design, as well as the ability to tune IET in gas systems could allow for the control of collisional stabilization versus reaction in combustion systems which could allow for more efficient and/or cleaner combustion.

Acknowledgments

The authors would like to thank Bill Hase for all of his hard work and great insights on this project, and we regret that he could not see the final published paper since he passed away during the writing of this paper. Funding for this project was provided by the United States Air Force

Office of Research (C13-0027), Air Force Office of Scientific Research under AFOSR Award Nos. FA9550-12-1-0443, FA9550-16-0133, and FA9550-17-1-0107, and the Robert A. Welch Foundation under Grant No. D-0005. Support was also provided by the High-Performance Computing Center (HPCC) at Texas Tech University, under the direction of Philip W. Smith. Parts of the computations were also performed on Robinson, a general computer cluster of the Department of Chemistry and Biochemistry, Texas Tech University, purchased by the NSF-CRIF-MU Grant No. CHE-0840493. A.K.P. also acknowledges SERB-DST, under file no. ECR/2017/001434 and CSIR under file no. 01 (2998)/19/EMR-II. SSA thanks NIT Meghalaya and MHRD for his fellowship. Parts of this paper were adapted from the thesis: West, N. Characterization of Benzene Laser-induced Nonthermal Equilibrium via Nitric Oxide Laser Induced Fluorescence Temperature Measurements. Texas A&M University, College Station, Texas, 2018. with permission from N.A.W.

Data Availability

Some of the data that supports the findings of this study are available within the article and its supplementary material in terms of plots. However, all the numerical data are available from the corresponding author upon reasonable request.

Appendix: Intermolecular Energy Transfer from a Vibrationally Excited Benzene Molecule in a Mixed Nitrogen-Benzene Bath

The negative of the decrease in the energy of the vibrationally excited benzene molecule, Bz^* , versus time is equal to the sum of the increase in the average energies of the benzene and nitrogen molecules in the bath versus time; i.e.

$$\frac{d\langle E(t) \rangle_{Bz^*}}{dt} = \frac{d\langle E(t) \rangle_{Bz}}{dt} + \frac{d\langle E(t) \rangle_{N_2}}{dt} \quad (A1)$$

The total collision frequency for Bz^* is a sum of its collision frequencies with the Bz and N_2 molecules in the bath; i.e.

$$\omega = \omega(Bz^* - Bz) + \omega(Bz^* - N_2) \quad (A2)$$

The average energy transfer from Bz^* per-collision, $\langle \Delta E_c \rangle_{Bz^*}$, is given by the left-side of Eq. (A3) and may be written as the properly weighted sum of the average energy transfers per collision to Bz and N_2 molecules in the bath as given by Eq. (A5); i.e.

$$\frac{1}{\omega} \frac{d\langle E(t) \rangle_{Bz^*}}{dt} = \frac{1}{\omega} \frac{d\langle E(t) \rangle_{Bz}}{dt} + \frac{1}{\omega} \frac{d\langle E(t) \rangle_{N_2}}{dt} \quad (A3)$$

$$\langle \Delta E_c \rangle_{Bz^*} = \frac{\omega(Bz^* - Bz)}{\omega} \frac{1}{\omega(Bz^* - Bz)} \frac{d\langle E(t) \rangle_{Bz}}{dt} + \frac{\omega(Bz^* - N_2)}{\omega} \frac{1}{\omega(Bz^* - N_2)} \frac{d\langle E(t) \rangle_{N_2}}{dt} \quad (A4)$$

$$\langle \Delta E_c \rangle_{Bz^*} = \frac{\omega(Bz^* - Bz)}{\omega} \langle \Delta E_c \rangle_{Bz} + \frac{\omega(Bz^* - N_2)}{\omega} \langle \Delta E_c \rangle_{N_2} \quad (A5)$$

The average energy transfer per collision to a Bz molecule in the bath is then

$$\langle \Delta E_c \rangle_{Bz} = \frac{\omega}{\omega(Bz^* - Bz)} \langle \Delta E_c \rangle_{Bz^*} - \frac{\omega(Bz^* - N_2)}{\omega(Bz^* - Bz)} \langle \Delta E_c \rangle_{N_2} \quad (\text{A6})$$

References

1. D. C. Tardy and B. S. Rabinovitch, *Chem. Rev.* **77**, 369 (1997).
2. G. Richmond and D. W. Setser, *J. Phys. Chem.* **84**, 2699 (1980).
3. H. Hippler, J. Troe, and H. J. Wendelken, *J. Chem. Phys.* **78**, 6709 (1983).
4. J. R. Barker and B. M. Toselli, *Int. Rev. Phys. Chem.* **12**, 305 (1993).
5. M. L. Yerram, J. D. Brenner, K. D. King, and J. R. Barker, *J. Phys. Chem.* **94**, 6341 (1990).
6. A. K. Paul, N. A. West, J. D. Winner, R. D. W. Bowersox, S. W. North, and W. L. Hase, *J. Chem. Phys.* **149**, 134101 (2018).
7. A. N. West, J. D. Winner, R. D. W. Bowersox, and S. W. North, *J. Chem. Phys.* **145**, 014308 (2016).
8. C. A. Michaels, A. S. Mullin, J. Park, J. Z. Chou, and G. W. Flynn, *J. Chem. Phys.* **108**, 2744 (1998).
9. K. F. Lim and R. G. Gilbert, *J. Phys. Chem.* **94**, 77 (1990).
10. I. Oref, O. Herscovitz, and E. Tzidoni, *J. Chem. Phys.* **87**, 98 (1983).
11. T. Lenzer, K. Luther, K. Reihls, and A. C. Symonds, *J. Chem. Phys.* **112**, 4090 (2000).
12. T. Lenzer and K. Luther, *J. Chem. Phys.* **104**, 3391 (1996).
13. D. A. Donzis, and A. F. Maqui, *J. Fluid Mech.* **797**, 181 (2016).
14. A. K. Paul, D. A. Donzis, and W. L. Hase, *J. Phys. Chem. A* **121**, 4049 (2017).
15. T. J. Fuller, A. G. Hsu, R. Sanchez-Gonzalez, J. C. Dean, S. W. North, and R. D. W. Bowersox, *The Journal of Fluid Mechanics* **748**, 663 (2014).
16. S. Khurshid and D. A. Donzis, *Phys. Fluids* **31**, 015103 (2019).

17. Leyva, S. Laurence, A. Beierholm, H. Hornung, R. Wagnild, and G. Candler, in *47th AIAA Aerospace Sciences Meeting including The New Horizons Forum and Aerospace Exposition* (American Institute of Aeronautics and Astronautics, 2009).
18. R. Wagnild, G. Candler, I. Leyva, J. Jewell, and H. Hornung, in *48th AIAA Aerospace Sciences Meeting Including the New Horizons Forum and Aerospace Exposition* (American Institute of Aeronautics and Astronautics, 2010).
19. R. Wagnild, G. Candler, P. Subbareddy, and H. Johnson, in *50th AIAA Aerospace Sciences Meeting including the New Horizons Forum and Aerospace Exposition* (American Institute of Aeronautics and Astronautics, 2012).
20. J. Jewell, R. Wagnild, I. Leyva, G. Candler, and J. Shepherd, in *51st AIAA Aerospace Sciences Meeting including the New Horizons Forum and Aerospace Exposition* (American Institute of Aeronautics and Astronautics, 2013).
21. A. V. Fedorov, V. Soudakov, and I. A. Leyva, in *7th AIAA Theoretical Fluid Mechanics Conference* (American Institute of Aeronautics and Astronautics, 2014).
22. B. E. Schmidt, and J. Shepherd, in *54th AIAA Aerospace Sciences Meeting* (American Institute of Aeronautics and Astronautics, 2016).
23. W. Liao, Y. Peng, and L-S. Luo, *Phys. Rev. E* **81**, 046704 (2010).
24. Z. Li, R. Sansom, S. Bonella, D. F. Coker, and A. S. Mullin, *J. Phys. Chem. A*, **109**, 7657 (2005)
25. M. Bruehl and G. C. Schatz, *J. Chem. Phys.* **89**, 770 (1988).
26. M. Bruehl and G. C. Schatz, *J. Phys. Chem.* **92**, 7223 (1988).
27. M. Bruehl and G. C. Schatz, *J. Chem. Phys.* **92**, 6561 (1990).
28. G. Lendvay and G. C. Schatz, *J. Phys. Chem.* **95**, 8748 (1991).

29. G. Lendvay and G. C. Schatz, *J. Chem. Phys.* **96**, 4356 (1992).
30. G. Lendvay and G. C. Schatz, *J. Chem. Phys.* **98**, 1034 (1993).
31. G. C. Schatz and G. Lendvay, *J. Chem. Phys.* **106**, 3548 (1997).
32. J. R. Barker, L. M. Yoder, and K. D. King, *J. Phys. Chem. A* **105**, 796 (2001).
33. J.-M. Zellweger, T. C. Brown, and J. R. Barker, *J. Chem. Phys.* **83**, 6251 (1985).
34. K. F. Lim and R. G. Gilbert, *J. Chem. Phys.* **84**, 6129 (1986).
35. K. F. Lim and R. G. Gilbert, *J. Chem. Phys.* **92**, 1819 (1990).
36. D. L. Clarke, I. Oref, R. G. Gilbert, and K. F. Lim, *J. Chem. Phys.* **96**, 5983 (1992).
37. D. L. Clarke and R. G. Gilbert, *J. Phys. Chem.* **96**, 8450 (1992).
38. A. K. Paul, S. C. Kohale, S. Pratihar, R. Sun, S. W. North, and W. L. Hase, *J. Chem. Phys.* **140**, 194103 (2014).
39. A. K. Paul, S. C. Kohale, and W. L. Hase, *J. Phys. Chem. C* **119**, 14683 (2015).
40. H. Kim, A. K. Paul, S. Pratihar, and W. L. Hase, *J. Phys. Chem. A* **120**, 5187 (2016).
41. H. Kim, B. Saha, S. Pratihar, M. Majumder, and W. L. Hase, *J. Phys. Chem. A* **121**, 7494 (2017).
42. H. Kim, H. N. Bhandari, S. Pratihar, and W. L. Hase, *J. Phys. Chem. A* **123**, 2301 (2019).
43. L. A. Rivera-Rivera, A. F. Wagner, T. D. Sewell, and D. L. Thompson, *J. Chem. Phys.* **142**, 014303 (2015).
44. R. Chitsazi and A. F. Wagner, *J. Chem. Phys.* **150**, 114303 (2019)
45. L. A. Rivera-Rivera, A. F. Wagner, and J. W. Perry, *J. Chem. Phys.* **151**, 034303 (2019).
46. N. West, Characterization of Benzene Laser-induced Nonthermal Equilibrium via Nitric Oxide Laser Induced Fluorescence Temperature Measurements. Doctoral dissertation, Texas A&M University, College Station, Texas, 2018.

47. W. L. Jorgensen and D. L. Severance, *J. Am. Chem. Soc.* **112**, 4768 (1990).
48. X. Ma, A. K. Paul, and W. L. Hase, *J. Phys. Chem. A* **119**, 6631 (2015).
49. E. C. Lee, D. Kim, P. Jurečka, P. Tarakeshwar, P. Hobza, and K. S. Kim, *J. Phys. Chem. A*, **111**, 3446 (2007).
50. V. Laporta, R. Celiberto, and J. M. Wadehra, *Plasma Sources Sci. Technol.* **21**, 055018 (2012).
51. S. Kolakkandy, A. K. Paul, S. Pratihari, S. C. Kohale, G. L. Barnes, H. Wang, and W. L. Hase, *J. Chem. Phys.* **142**, 044306 (2015).
52. A. K. Paul, S. Kolakkandy, and W. L. Hase, *J. Phys. Chem. A* **119**, 7894 (2015).
53. T. Lenzer, K. Luther, J. Troe, R. G. Gilbert, and K. F. Lim, *J. Chem. Phys.* **103**, 626 (1995).
54. W. L. Hase and D. G. Buckowski, *Chem. Phys. Lett.* **74**, 284 (1980).
55. G. H. Peslherbe, H. Wang, and W. L. Hase, *Adv. Chem. Phys.* **105**, 171 (1999).
56. X. Hu, W. L. Hase, and T. Pirraglia, *J. Comput. Chem.* **12**, 1014 (1991).
57. D. C. Clary, R. G. Gilbert, V. Bernshtein, and I. Oref, *Faraday Discuss.* **102**, 423 (1995)
58. V. Bernshtein and I. Oref, *J. Phys. Chem. B* **109**, 8310 (2005).
59. S. Hamon, S. D. Le Picard, A. Canosa, B. R. Rowe, and I. W. M. Smith, *J. Chem. Phys.* **112**, 4506 (2000).
60. J. D. Winner, N. A. West, M. H. McIlvoy, Z. D. Buen, R. D. Bowersox, and S. W. North, *J. Chem. Phys.* **501**, 86 (2018).
61. S. S. Ahamed, H. Mahanta, and A. K. Paul, *J. Phys. Chem. A* **123**, 10663 (2019).

Table I. Molecular temperatures at the end of the 3 ps simulation^a

<u>Molecule</u>	<u>T_{trans}</u>	<u>T_{rot}</u>	<u>T_{vib}</u>
C ₆ H ₆ *	164	225	855
C ₆ H ₆	150	188	543
N ₂	158	157	140

a. These are temperatures (K) for the N₂/C₆H₆ bath initially at 140 K. The initial C₆H₆* translational/rotational temperature is 300 K, whereas, the initial vibrational temperature of C₆H₆* is 2484 K, corresponding to the classical excitation energy of 148.1 kcal/mol.

Table II. Conditions and Fitting Parameters for Four Simulations of $\langle E(t) \rangle$

Bath ^a				Fit parameters ^b					
T	P	N ₂	C ₆ H ₆	$E(0)$	$E(\infty)$	f_1	f_2	k_1	k_2
300 ^c	32.5	190	9	149.9	23.4	0.901	0.089	1.33×10^{-3}	7.99×10^{-4}
140	16.2	396	4	149.0	12.2	0.600	0.400	7.24×10^{-4}	1.98×10^{-4}
300	35.0	400	0	149.5	19.8	0.998	0.002	1.33×10^{-4}	1.30×10^{-4}
140	16.3	399	0	149.0	51.9	0.600	0.400	1.74×10^{-4}	5.60×10^{-5}

a. Temperature (K,) pressure (atm) of the bath, and the number of N₂ and C₆H₆ molecules in the bath

b. $E(0)$ and $E(\infty)$ are in kcal/mol, $f_1 + f_2 = 1$, and k_1 and k_2 are in ps⁻¹.

c. These parameters are collected from ref. 6.

Table III. Partial Pressures and Collision Frequency Parameters for Two Mixed Bath Simulations at 140 and 300 K

Bath ^a			Frequency parameters ^b			
<i>T</i>	P(N ₂)	P(C ₆ H ₆)	ω_P (N ₂)	ω_P (C ₆ H ₆)	ω (C ₆ H ₆ *- C ₆ H ₆)	ω (C ₆ H ₆ *- N ₂)
300	31.0	1.5	1.14 x 10 ¹⁰	1.74 x 10 ¹⁰	2.58 x 10 ¹⁰	3.53 x 10 ¹¹
140	16.1	0.12	2.41 x 10 ¹⁰	3.68 x 10 ¹⁰	4.49 x 10 ⁹	3.87 x 10 ¹¹

- a. The partial pressures are given in atm.
- b. ω_P values are written in atm⁻¹ s⁻¹, and ω values are in s⁻¹

Figure Captions

FIG. 1. Results for the N_2/C_6H_6 bath simulation at 140 K. Plot of center-of-mass distance between two benzene molecules versus time for the trajectory where the probability of complex formation is minimum: (a) Bz1-Bz2; (b) Bz1-Bz3; (c) Bz1-Bz4; (d) Bz2-Bz3; (e) Bz2-Bz4; and (f) Bz3-Bz4. Bz1 is $C_6H_6^*$ and Bz2, Bz3, and Bz4 are the 3 C_6H_6 molecules in the bath. The dotted line in each panel is drawn at the center-of-mass distance of 10 Å.

FIG. 2. Same as Fig. 1, but for the trajectory where the probability of complex formation is maximum: (a) Bz1-Bz2; (b) Bz1-Bz3; (c) Bz1-Bz4; (d) Bz2-Bz3; (e) Bz2-Bz4; and (f) Bz3-Bz4. Bz1 is $C_6H_6^*$ and Bz2, Bz3, and Bz4 are the 3 C_6H_6 molecules in the bath. The dotted line in each panel is drawn at the center-of-mass distance of 10 Å.

FIG. 3. Result for the N_2/C_6H_6 bath simulation at 140 K. Total energy of the excited benzene molecule $C_6H_6^*$ versus time.

FIG. 4. Results for the N_2/C_6H_6 bath simulation at 140 K. Average translation (red) and rotation (green) energies of C_6H_6 (top panel) and N_2 (bottom panel) bath molecules versus time, and vibration (black) energy of a N_2 bath molecule and a vibration mode of a C_6H_6 bath molecule versus time.

FIG. 5. $C_6H_6^*$ energies for the N_2/C_6H_6 bath simulation at 140 K. Average translation (red) and rotation (green) energies, and, energy of a vibration mode (black) versus time.

FIG. 6. Results for the N₂ bath simulations at 140 K in panel (a) and 300 K in panel (b). Total energy of the excited benzene molecule C₆H₆* versus time. The black curve is the simulation and the red curve is the fit.

FIG. 7. Average energies transferred to the N₂ and benzene bath molecules, i.e., $\langle \Delta E_c \rangle_{Bz}$ (top panel) and $\langle \Delta E_c \rangle_{N_2}$ (bottom panel), from vibrationally excited C₆H₆*, for the simulations at 140 K and 300 K. Results are given versus the average vibrational energy of C₆H₆*.

FIG. 8. Values of $\langle \Delta E_c \rangle$ versus $\langle E \rangle$ of C₆H₆* for N₂/C₆H₆ baths at 140 and 300 K. Results are given for two bath compositions. Bath with 9 C₆H₆ and 190 N₂ (top panel), $\langle \Delta E_c \rangle$ at 140 K (black) and 300 K (red); bath with 3 C₆H₆ and 396 N₂ (bottom panel), $\langle \Delta E_c \rangle$ at 140 K (black) and 300 K (red). The same curve for 140 K experiment, as obtained from ref. 46, is presented in the inset of the latter panel.

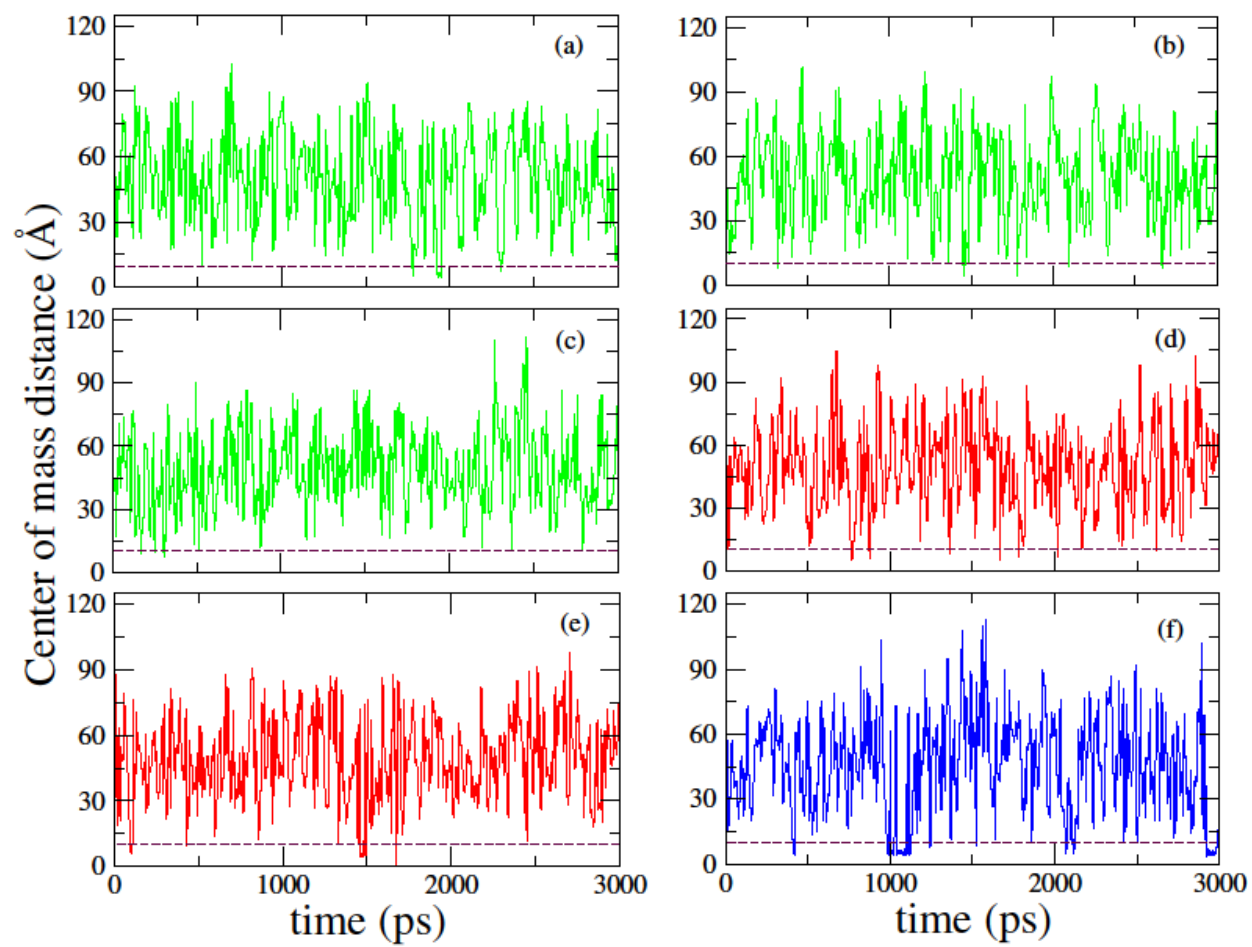


FIG. 1

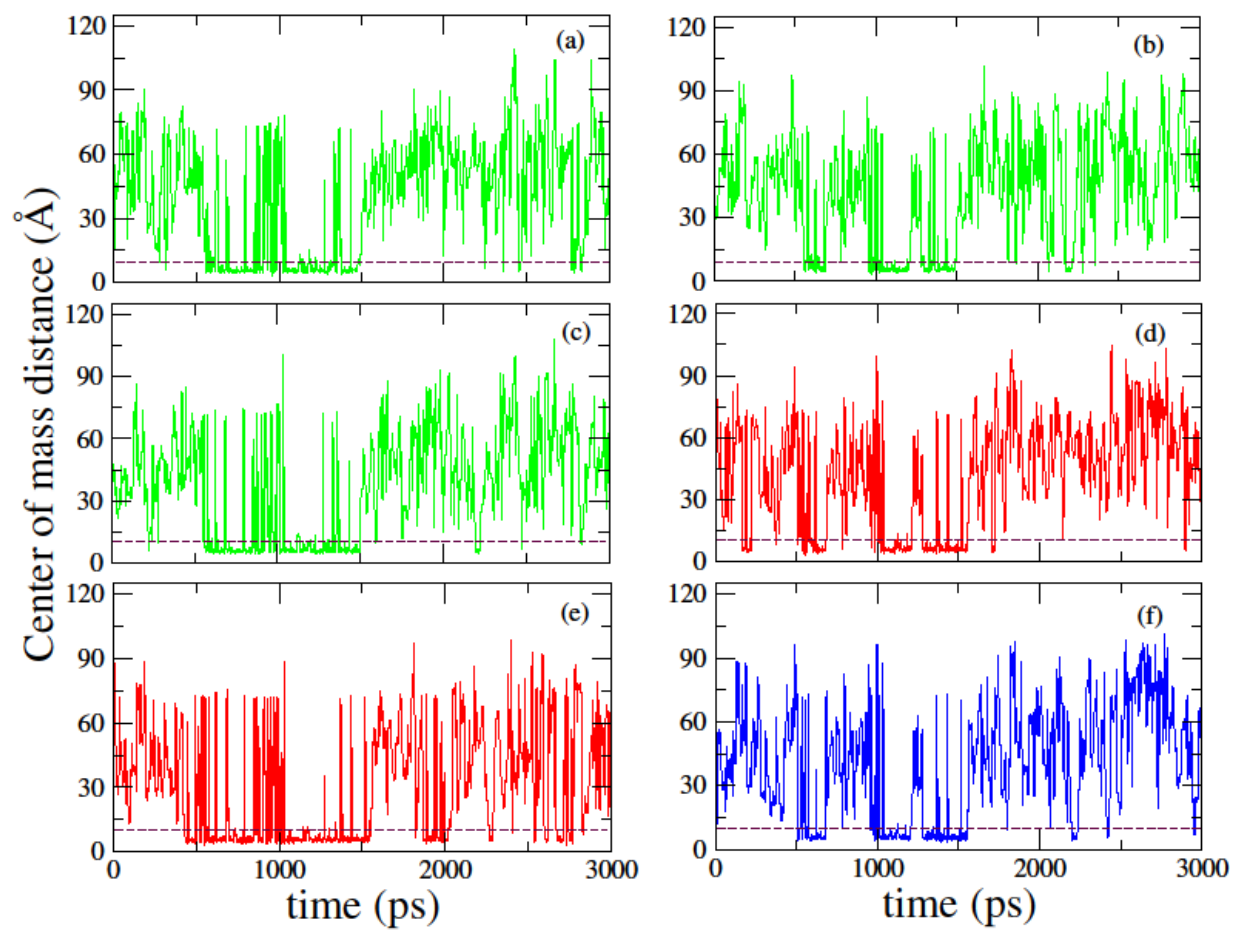


FIG. 2

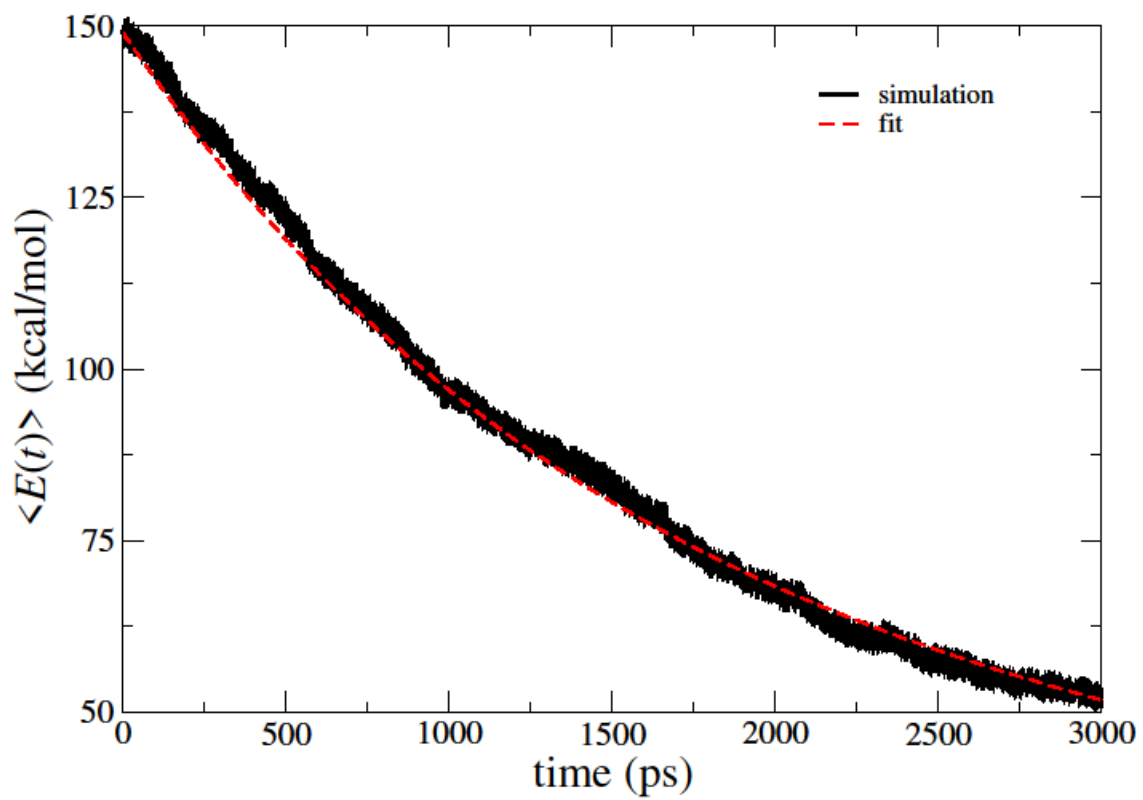


FIG. 3

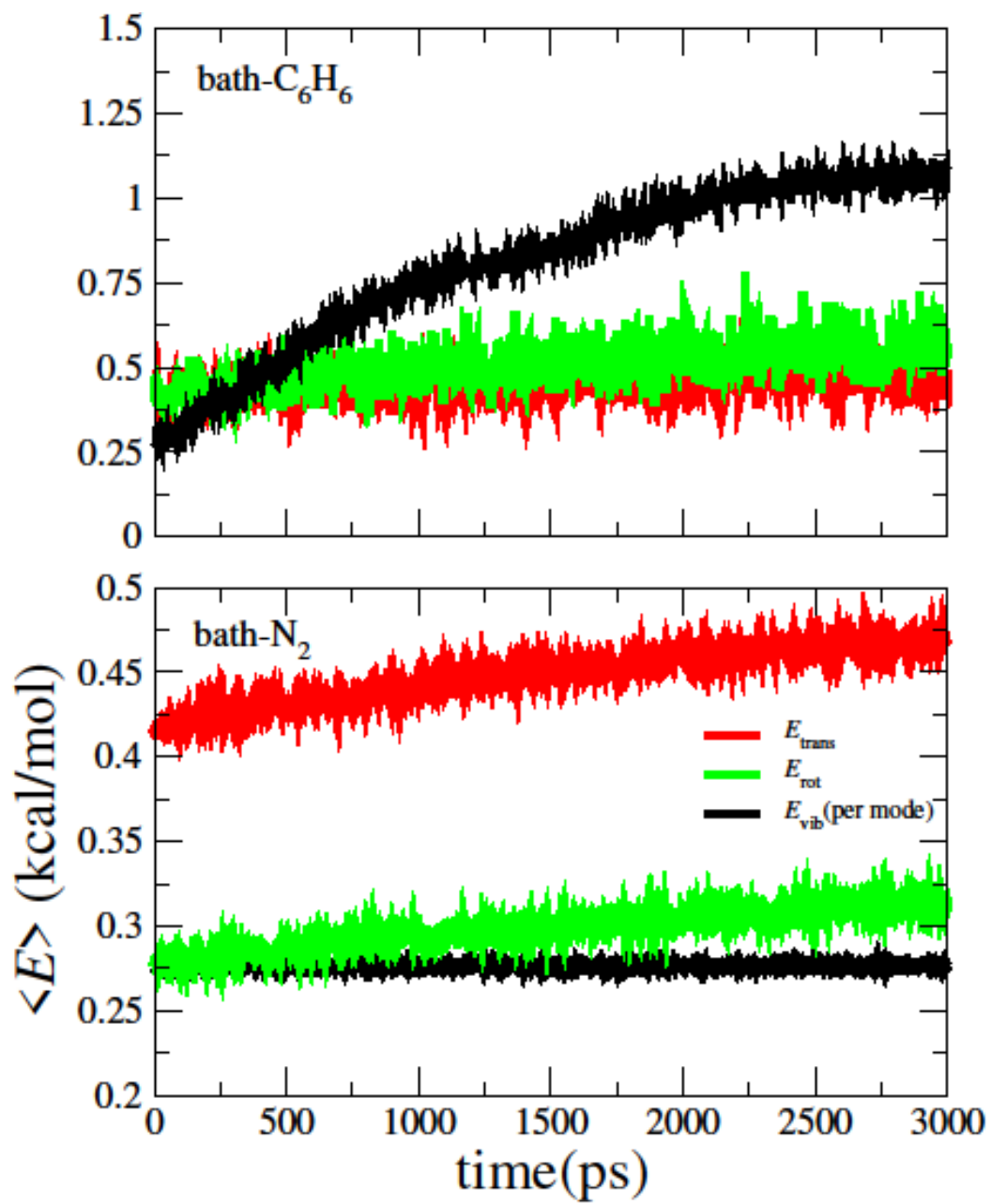


FIG. 4

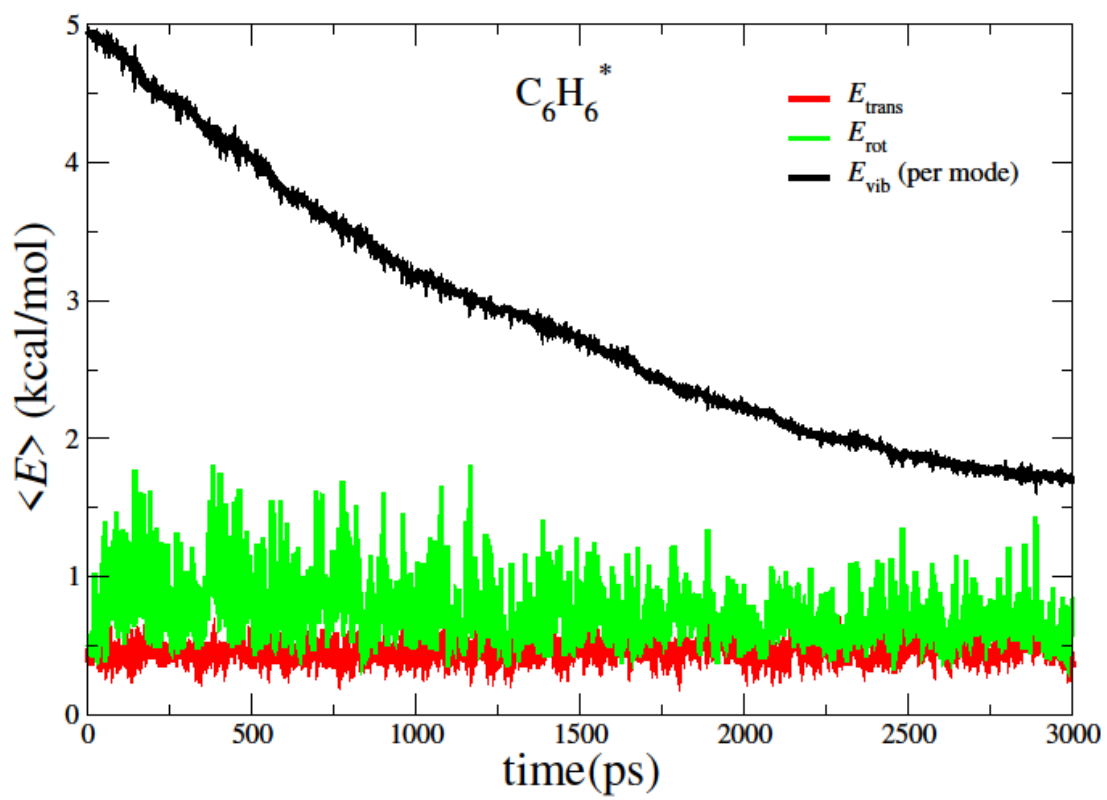


FIG. 5

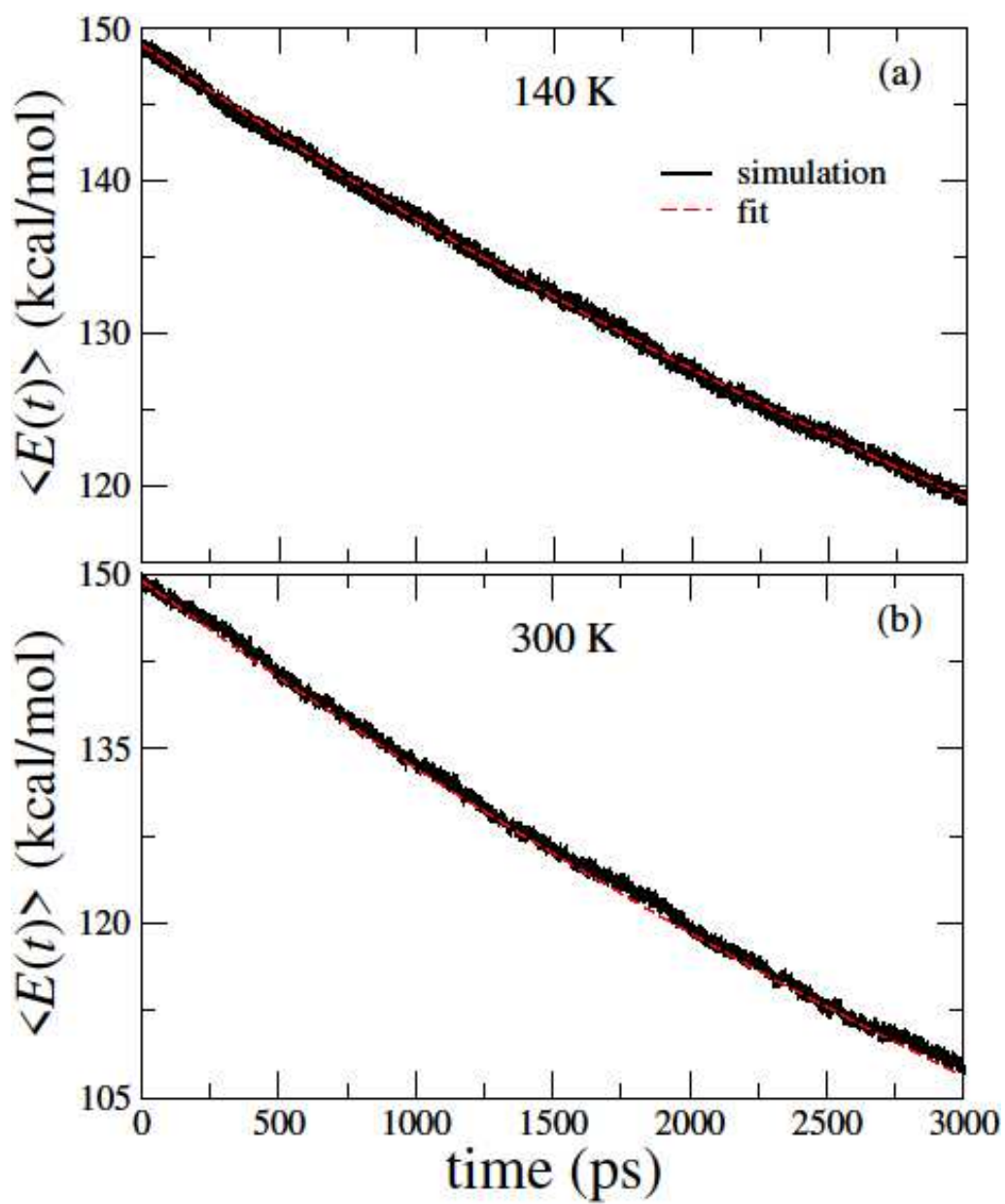


FIG. 6

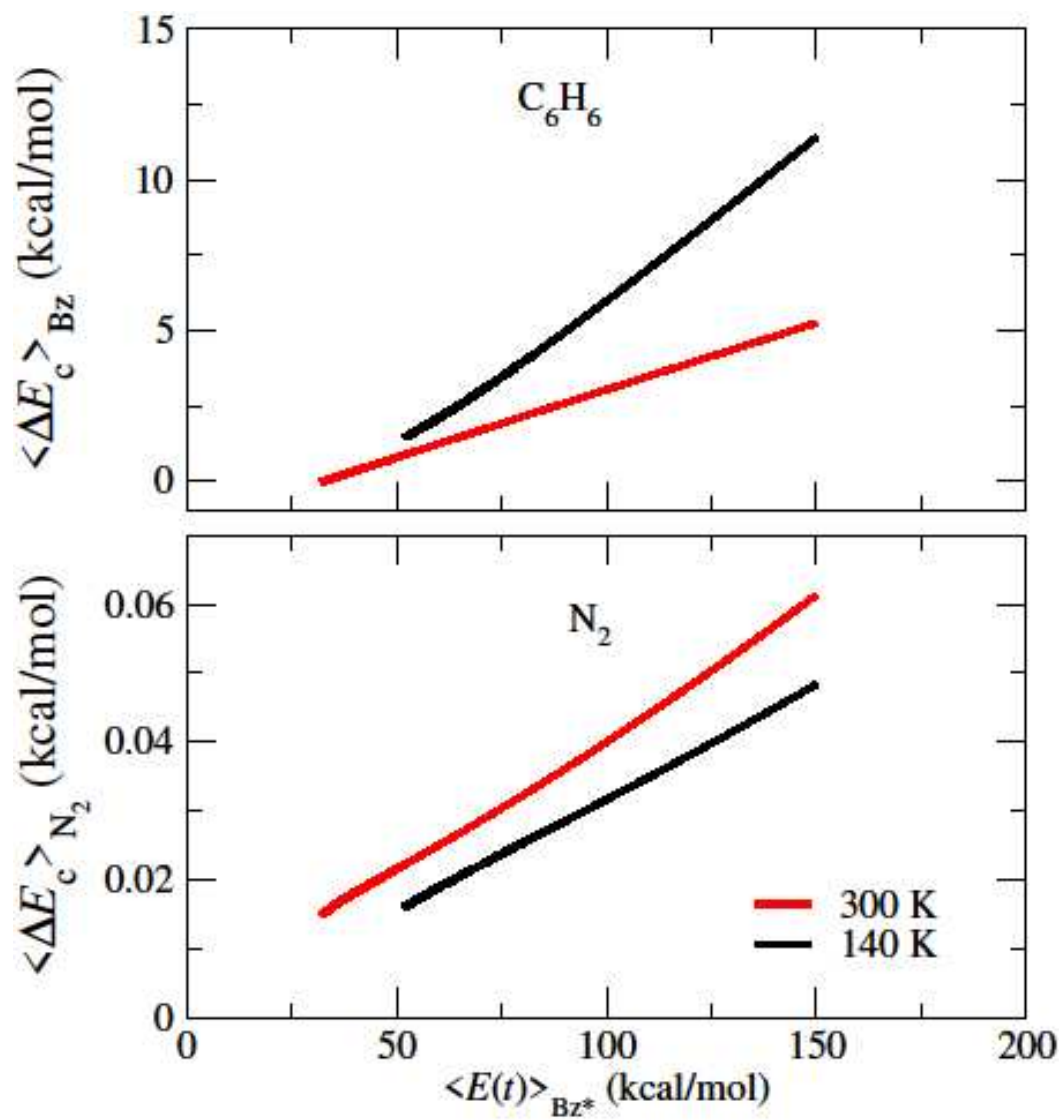


FIG. 7

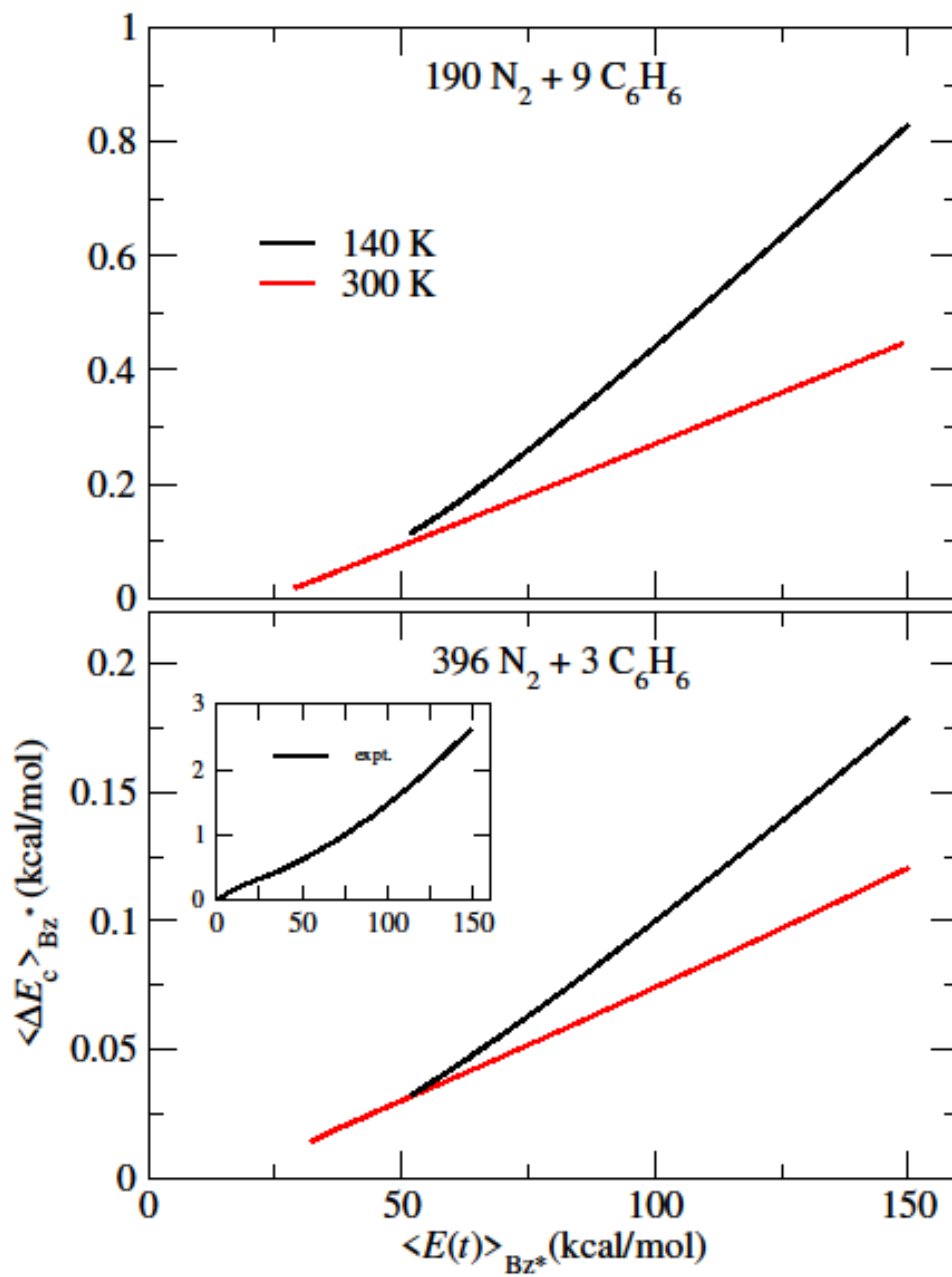


FIG. 8